

# Detection of two power-law tails in the probability distribution functions of massive GMCs

N. Schneider,<sup>1,2★</sup> S.Bontemps<sup>1</sup>, P.Girichidis<sup>3</sup>, T.Rayner<sup>4</sup>, F.Motte<sup>5</sup>, Ph.André<sup>5</sup>, D.Russeil<sup>6</sup>, A.Abergel<sup>7</sup>, L.Anderson<sup>8</sup>, D.Arzoumanian<sup>7</sup>, M.Benedettini<sup>9</sup>, T.Csengeri<sup>10</sup>, P.Didelon<sup>5</sup>, J.Di Francesco<sup>11</sup>, M.Griffin<sup>4</sup>, T.Hill<sup>12</sup>, R.S.Klessen<sup>13</sup>, V.Ossenkopf<sup>2</sup>, S.Pezzuto<sup>9</sup>, A.Rivera-Ingraham<sup>14</sup>, L.Spinoglio<sup>9</sup>, P.Tremblin<sup>15,5</sup>, A. Zavagno<sup>5</sup>

<sup>1</sup>*OASU/LAB Univ. Bordeaux, CNRS, UMR5804, 33270 Floirac, France*

<sup>2</sup>*I. Physik. Institut, University of Cologne, 50937 Cologne, Germany*

<sup>3</sup>*Max Planck Institut für Astrophysik, 85741 Garching, Germany*

<sup>4</sup>*School of Physics and Astronomy, Cardiff University, CF24 3AA, UK*

<sup>5</sup>*IRFU/Sap CEA/DSM, Lab. AIM CNRS - Université Paris Diderot, 91191 Gif-sur-Yvette, France*

<sup>6</sup>*AIX Marseille Univ. LAM, CNRS, UMR 7326, 13388 Marseille, France*

<sup>7</sup>*IAS, CNRS, UMR8617, Université Paris Sud, 91400 Orsay, France*

<sup>8</sup>*Department of Physics and Astronomy, West Virginia University, WV 26506, USA*

<sup>9</sup>*IAPS, INAF, 00133 Roma, Italy*

<sup>10</sup>*Max Planck Institut für Radioastronomie, 53121 Bonn, Germany*

<sup>11</sup>*NRC, Herzberg Institute of Astrophysics, Victoria, Canada*

<sup>12</sup>*Joint ALMA Observatory, Santiago, Chile*

<sup>13</sup>*Universität Heidelberg, Zentrum für Astronomie, 69120 Heidelberg, Germany*

<sup>14</sup>*ESA/ESAC, Madrid, Spain*

<sup>15</sup>*Astrophysics Group, University of Exeter, UK*

Accepted 2015 July 21. Received 2015 July 20; in original form 2015 June 29

## ABSTRACT

We report the novel detection of complex high-column density tails in the probability distribution functions (PDFs) for three high-mass star-forming regions (CepOB3, MonR2, NGC6334), obtained from dust emission observed with *Herschel*. The low column density range can be fit with a lognormal distribution. A first power-law tail starts above an extinction ( $A_V$ ) of  $\sim 6$ –14. It has a slope of  $\alpha=1.3$ –2 for the  $\rho \propto r^{-\alpha}$  profile for an equivalent density distribution (spherical or cylindrical geometry), and is thus consistent with free-fall gravitational collapse. Above  $A_V \sim 40$ , 60, and 140, we detect an excess that can be fitted by a flatter power law tail with  $\alpha > 2$ . It correlates with the central regions of the cloud (ridges/hubs) of size  $\sim 1$  pc and densities above  $10^4$  cm<sup>-3</sup>. This excess may be caused by physical processes that slow down collapse and reduce the flow of mass towards higher densities. Possible are: 1. rotation, which introduces an angular momentum barrier, 2. increasing optical depth and weaker cooling, 3. magnetic fields, 4. geometrical effects, and 5. protostellar feedback. The excess/second power-law tail is closely linked to high-mass star-formation though it does not imply a universal column density threshold for the formation of (high-mass) stars.

**Key words:** ISM:clouds

## 1 INTRODUCTION

Probability distribution functions (PDFs) of column density  $N(\text{HI}+\text{H}_2)$  obtained using far-infrared emission of dust

from *Herschel*<sup>1</sup> show a characteristic shape for low-mass star-forming regions: a lognormal distribution for low  $N$ , commonly attributed to turbulence, and a single power-law

<sup>1</sup> *Herschel* is an ESA space observatory with science instruments provided by European-led Principal Investigator consortia and with important participation from NASA.

★ E-mail: nicola.schneider@obs.u-bordeaux1.fr

tail for higher  $N$  (e.g., Schneider et al. 2013, and references therein). This sort of PDF is also found for extinction maps (Kainulainen et al. 2009; Froebrich & Rowles 2010). There is an ongoing discussion whether this power-law tail can be attributed to self-gravity (Klessen 2000; Kritsuk et al. 2011; Federrath & Klessen 2013; Girichidis et al. 2014; Schneider et al. 2013, 2015a) or is pressure-driven (Kainulainen et al. 2011).

In this *Letter*, we show that PDFs obtained from *Herschel* dust column density maps of giant molecular clouds (GMCs) not only show a clear lognormal plus power-law tail distribution but can also exhibit an excess at very high column densities that can be identified as a second, shallower power law. It seems that this discovery is restricted to the densest regions of massive molecular clouds (ridges/hubs), though not all those GMCs display this feature. The objective of this study is to report our detection and give some tentative explanations for its existence.

## 2 OBSERVATIONS

We make use of *Herschel*-derived column density ( $N$ ) PDFs of three well-known GMCs. Data and PDFs of MonR2 at a distance of 0.83 kpc (Rayner et al., in prep, Didelon et al. 2015) and NGC6334 at a distance of 1.35 kpc (Russeil et al. 2013) were obtained within the HOBYS (*Herschel* imaging survey of OB Young Stellar objects) key program (Motte et al. 2010), while the data for CepOB3 (distance 0.7 kpc, PI Gutermuth) were taken from the *Herschel* (Pilbratt et al. 2010) archive. We selected these sources as examples because they cover different ranges in distance, mass, and UV-field (Table 1). Dust optical depths and temperatures were determined from a greybody fit to the surface brightness at the 160  $\mu\text{m}$  wavelength of PACS (Poglitsch et al. 2010) together with the 250, 350, and 500  $\mu\text{m}$  wavelengths of SPIRE (Griffin et al. 2010). For that, we assume a constant line-of-sight temperature for each pixel. The optical depths are then converted into  $\text{H}_2$  column densities taking a dust opacity  $\kappa_\lambda = 0.1 \times (\lambda/300\mu\text{m})^{-\beta} \text{ cm}^2/\text{g}$  with a fixed  $\beta=2$ . Opacity variations were observed in Orion A (Roy et al. 2014) so that we arrive to a relative accuracy of  $\sim 50\%$  over the whole column density range covered in *Herschel* observations. For more details, we refer to Hill et al. (2011), Schneider et al. (2015a), and Könyves et al. (2015). For CepOB3, the PACS 160  $\mu\text{m}$  data contain nonfunctional bolometers. The resulting column density maps thus show a regular pattern with missing points, so that we fitted only the 250, 350, and 500  $\mu\text{m}$  data points. The angular resolution of the maps is  $36''$ , matched to the longest-wavelength *Herschel* band.

## 3 PROBABILITY DISTRIBUTION FUNCTIONS OF GMCS

Figure 1 shows the column density maps and corresponding PDFs for the GMCs of our study. To describe the PDF, we use the notation  $p(\eta)$  with

$$p(\eta)d\eta = (2\pi\sigma_\eta^2)^{-0.5} \exp[-(\eta-\mu)^2/(2\sigma_\eta^2)]d\eta \quad (1)$$

with  $\eta = \ln(N/\langle N \rangle)$ ,  $\sigma_\eta$  as the dimensionless dispersion of the logarithmic field, and  $\mu$  as the mean. We determine  $\sigma_\eta$  with a fit to the assumed lognormal low column density part of the PDF and the slopes from a linear regression power-law fit with  $p(\eta) = p_0(\eta/\eta_0)^s$  to the high-density parts (see

Schneider et al. 2015a,b, for more details). The intersection between lognormal and power-law tail regime lies at extinctions<sup>2</sup>  $A_V$  of around 6–8 for CepOB3 and MonR2 and  $A_V \sim 14$  for NGC6334. Starting at these values, we then fit a power-law to the distribution up to the break point where additional high  $A_V$  excess becomes apparent, i.e., at  $A_V \sim 40$  for MonR2,  $A_V \sim 60$  for CepOB3, and  $A_V \sim 140$  for NGC6334. This spread in values shows that the shift to a shallower power law does not represent a universal threshold such as the one proposed for massive star formation around  $A_V = 300$  (Krumholz & McKee 2008). The excess is clearly evident over a range of  $A_V \sim 40$ –200 for MonR2,  $A_V \sim 60$ –200 for CepOB3, and  $A_V \sim 140$ –300 for NGC6334. Although it can be fitted by a power-law<sup>3</sup>, we cannot exclude the possibility that other distributions can fit the excess similarly well. In considering its physical interpretation in comparison to the first power-law tail, we keep the premise of a second power-law.

A word of caution is appropriate with regard to the PDF shape. Additional extinction due to foreground/background emission provokes that the width of the lognormal part becomes more narrow and the peak shifts to higher  $A_V$ , while the slope(s) of the power-law tail(s) are steeper, compared to an undisturbed distribution (Schneider et al. 2015a). However, the slope of the second power-law tail is less affected because a contamination of a few  $A_V$  does not significantly change the highest column densities. Contamination and projection effects, however, could still lead to substructure in the PDF, which might complicate the simple lognormal + power-law tail(s) representation. The accuracy of the lognormal fit is thus limited and the first deviation point is not well defined.

## 4 SPATIAL IDENTIFICATION OF THE DIFFERENT PDF REGIMES

To identify the pixels that constitute the two power-law tails, we outline in Fig. 1 with a red and yellow contour the respective  $A_V$ -thresholds. While the red contour traces mainly filaments, the yellow contour encloses individual *clumps* with a size scale of  $\sim 1$  pc, delimiting single (MonR2) or several (CepOB3, NGC6334) star-forming center(s) of the GMCs. These central regions correspond in their geometry and physical properties to what was defined as ‘ridges’ (or hubs) in massive clouds (Hill et al. 2011; Hennemann et al. 2012), i.e., regions with high column density ( $N > 10^{23} \text{ cm}^{-2}$ ) over small areas. The PACS 70  $\mu\text{m}$  images (Fig. 1) indicate the stellar/protostellar activity in these clumps: NGC6334 contains several H II regions and a few ultra-compact (UC) H II regions (e.g., Russeil et al. 2013), MonR2 hosts several UC H II regions and bipolar outflows (e.g., Fuente et al. 2010; Dierickx et al. 2015), and CepOB3 includes an embedded massive cluster. Table 1 lists the masses contained above the two break points. For the high column density regime (yellow),

<sup>2</sup> For better comparison to other studies in the literature, we use the visual extinction value derived from the column density adopting  $N(\text{H}_2)/A_V = 0.94 \times 10^{21} \text{ cm}^{-2} \text{ mag}^{-1}$  (Bohlin et al. 1978).

<sup>3</sup> The reduced  $\chi^2_{\text{red}}$  values of the second power law fits scatter around unity ( $1.05 \pm 0.28$ ,  $1.08 \pm 0.10$ ,  $2.43 \pm 0.16$  for CepOB3, MonR2, NGC6334) indicating that the general assumption of a power-law dependence is justified.

**Table 1.** Properties of GMCs: total mass  $M$  derived above the first closed contour, i.e.  $A_V=2$  for CepOB3 and MonR2 and  $A_V=4$  for NGC6334, masses (the percentage of the total mass given in parenthesis) above the first (DP1) and second (DP2) deviation point in the PDF (values determined from the *Herschel* N-maps), average and maximum UV-flux in units of the Habing field (obtained from the *Herschel* fluxes (Roccatagliata et al. 2013)), slopes  $s_1/s_2$  of power-law tails, exponents  $\alpha_{s1/2}$  and  $\alpha_{c1/2}$  for a spherical and cylindrical density distribution, equivalent beam deconvolved radius  $r$  (taking an area  $A=\pi r^2$ ), and density  $n$ , determined from the average column density and  $r$  with  $n=N/(2r)$ . The values of  $r$  and  $n$  for NGC6334 are averages over several clumps. The errors of both  $\alpha_c$  and  $\alpha_s$  determined from the first slope are  $\sim 0.02$ , and those from the second slope are  $\sim 0.05$ .

	$M_{total}$ [ $10^4 M_\odot$ ]	$M(DP1)$ [ $10^4 M_\odot$ ]	$M(DP2)$ [ $10^4 M_\odot$ ]	$\langle UV \rangle$ [ $G_0$ ]	$UV_{max}$ [ $10^4 G_0$ ]	$s_1$	$s_2$	$\alpha_{s1}$	$\alpha_{c1}$	$\alpha_{s2}$	$\alpha_{c2}$	$r$ [pc]	$\langle n \rangle$ [ $10^4 \text{ cm}^{-3}$ ]
CepOB3	10.0	1.7 (17%)	0.052 (0.5%)	40	8.0	-3.80	-1.18	1.53	1.26	2.70	1.85	0.29	6.0
MonR2	1.4	0.54 (39%)	0.21 (15%)	52	4.8	-2.10	-1.05	1.95	1.48	2.90	1.95	0.65	1.9
NGC6334	23.1	7.3 (32%)	3.53 (15%)	302	8.9	-2.26	-0.61	1.88	1.44	4.17	2.64	0.42	34.7

we determine also the equivalent radius  $r$ , and the density  $n$ . It becomes obvious that most of the mass is constituted by the lower column density regime, i.e., 83%, 61%, and 68% for CepOB3, MonR2, and NGC6334, respectively. The mass above the first deviation point makes up 15% to 39% of the complexes. The highest column density clumps still account for a significant amount of mass in MonR2 and NGC6334 (both 15%), but a much smaller proportion ( $<1\%$ ) for CepOB3. The average density  $\langle n \rangle$  in these clumps is also high, i.e., between  $2 \times 10^4 \text{ cm}^{-3}$  and  $3.5 \times 10^5 \text{ cm}^{-3}$ . However, the existence of high density clumps/cores does not by itself explain the second power law. In a region such as Aquila,  $\sim 15\%$  of the total cloud mass resides in gas of density larger than  $10^4 \text{ cm}^{-3}$  (Könyves et al. 2015), but only a single power-law tail is observed (Schneider et al. 2013; André et al. 2014). We focus now on the analysis of the two power-law tails. From the slope  $s$ , the exponent  $\alpha$  for the density distribution  $\rho(r) \propto r^{-\alpha}$  can be derived. For a spherical geometry, representing clumps and cores,  $\alpha = -2/s + 1$  (Federrath & Klessen 2013). For a cylindrical one, characterizing filaments,  $\alpha = -1/s + 1$  (Myers 2015). Table 1 lists the values for both geometries for the first and second tail. The values of  $\alpha$  for the first tail range between 1.3 and 2, consistent with free-fall collapse, see Schneider et al. (2013, 2015a,b) and Girichidis et al. (2014) for a detailed discussion of both filaments and clumps/cores. The values of  $\alpha_{c2}$  between 1.85 and 2.64 correspond very well to the range of values directly measured for the B211/B213 filament in Taurus in Palmeirim et al. (2013). Independent observational support for gravitational contraction comes from molecular line observations of other GMCs that show spectral infall signatures across ridges (Schneider et al. 2010, 2015b; Galvan-Madrid et al. 2010; Peretto et al. 2013). These studies show that the formation of high-mass stars requires a very large mass accretion rate, provided by infall from merging filaments and gravitational collapse of larger structures on parsec-scales. For the excess – presuming it can be described by a power-law –  $\alpha$  lies between 1.9 and 4.2. The assumption of a spherical density distribution is probably more valid here, because the corresponding regions are more compact and circular. However, free-fall alone can not produce  $\alpha > 2$ , only a slowed-down collapse can lead to piling up high (column) densities on very small spatial scales.

## 5 SIGNIFICANCE OF THE EXCESS

The PDF excess we observe for the GMCs in our study is not a systematic property of all GMCs. It is also seen in Rosette (Schneider et al. 2012), W43 and W51 (Schneider et al., in prep.), and W3 (Rivera-Ingraham et al., 2015), but there is no example of a low-mass star-forming cloud that displays this feature. Similarly, there are also massive clouds such as Carina and NGC3603 (Schneider et al. 2015a), Vela (Hill et al. 2011), or M16 (Hill et al. 2012) where no clear indication for this excess is found in the PDFs of the whole cloud. Therefore, it is unlikely that the excess is caused by a systematic bias introduced during the determination of the dust column density maps.

It is out of the scope of this paper to discuss in detail the general uncertainties related to the determination of the column density maps and we refer the reader to Roy et al. (2013, 2014) and Könyves et al. (2015). Nevertheless, we mention here briefly the biases that could potentially influence the inferred slope and are thus relevant for the results of this paper: 1) An overestimation of the line-of-sight temperature (assumed to be constant for the SED fit) leads to an underestimation of the column density (and the vice versa). 2) If dust opacity increases towards high column densities, then this could give rise to a steeper slope of the power-law tail at higher densities. 3) The adopted value of the specific dust opacity  $\beta=2$  could be too high in parts of the warm GMCs. A lower (higher) value of  $\beta$  in the greybody fits leads to higher temperatures and thus lower (higher) column densities.

## 6 WHAT CAUSES THE TWO POWER-LAW TAILS IN THE PDF?

Given that the excess/second power-law tail is only found in high-density ( $\langle n \rangle \sim 10^4\text{--}5 \text{ cm}^{-3}$ ) star-forming clumps on size scales of  $\sim 1 \text{ pc}$ , i.e. in ridges/hubs, the physical process(es) in control of it must be active on small scales. It is evident that at these densities gravitational collapse of individual star-forming cores is involved, but it is not yet understood what produces the remarkable excess in column density.

We emphasize that in all cases the newly found excess is preceded by a first power-law in the PDF consistent with the dominant effect of self-gravity found by numerical simulations (e.g., Vazquez-Semadeni et al. 2008; Kritsuk et al. 2011) as well as observations (e.g., Schneider et al. 2013, 2015a,b). We thus expect the regions under consideration to

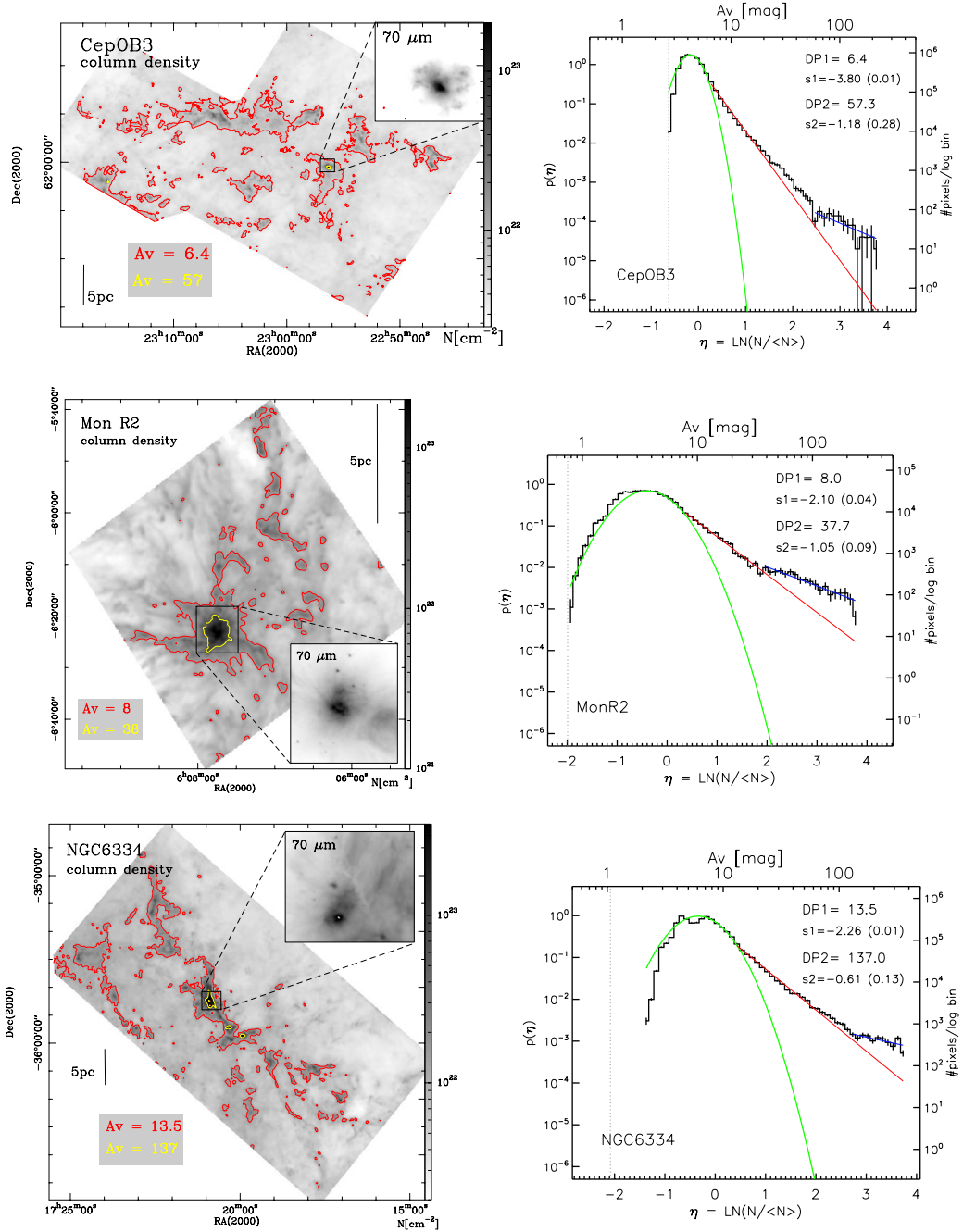


**Figure 1.** **Left:** Dust column density maps of the GMCs. Contour lines in red and yellow indicate the break points between the lognormal distribution and the first and second power-law tail, respectively. The small panels show a zoom into the central regions, displaying PACS 70  $\mu\text{m}$  emission (scale typically 0.1-30 Jy/pixel). **Right:** Corresponding PDFs at an angular resolution of 36'' (binsize 0.1). The left y-axis indicates the normalized probability  $p(\eta)$ , the right y-axis the number of pixels per logarithmic bin. The error-bars were calculated using Poisson-statistics. The upper x-axis gives the extinction  $A_v$  and the lower x-axis  $\eta = \ln(N/\langle N \rangle)$ . The green curve indicates the fitted lognormal PDF and the red and blue lines the power law fits to the high-density tails. The fit to the first tail was only performed between the break points but the line was continued to emphasize the excess. The deviation points (DP) and slopes ( $s$  with its error) of the power-law tails are given in each panel.

contract in almost free-fall (Girichidis et al. 2014), i.e., gas at a density  $\rho_i$  falls towards higher densities  $\rho'_i > \rho_i$ . Without any change in physical processes for higher densities, free-fall would proceed unimpeded and the power-law would extend indefinitely. Deviations from this idealised single power-law can be twofold. On the one hand the second excess could

be due to a change in dynamics at high densities or due to observational effects. In the following we give some tentative explanations that, however, need more profound studies.

Any physical process that slows down the free-fall motions reduces the flow of mass towards higher densities. We stress that in this paradigm the deceleration of free-fall stems



from *within* the centres of the cloud clumps. Processes acting from the outside like a hot ambient medium in which the cloud is embedded or large-scale colliding flows are unlikely to directly alter the PDF at the highest densities without altering the distribution at lower densities that is in the free-fall regime of the first power-law. Rotational effects (1.) have been invoked to explain excess at high densities seen in a density PDF obtained from an isothermal, self-gravitating supersonic turbulence simulation (Kritsuk et al. 2011). The spatial scales at which angular momentum is likely to dominate, however, are probably smaller than the resolution of the observations presented in this paper (0.1–0.25 pc). Likewise, thermodynamical effects of increasing thermal pressure due to shielding and reduced cooling (2.) is unlikely to dominate at the observed scales (e.g., Larson 2005). The role of magnetic fields (3.) is rather unclear. It was shown that *strong* (Koertgen et al. 2015) or *intermediate* (Heitsch et al. 2001) magnetic fields, acting on a clump scale, slow down and can even completely prevent the star-formation process in magneto-hydrodynamic (MHD) simulations. If magnetic fields entirely prevent the collapse and star formation, the clouds are stable and will not show a first gravitationally dominated power-law in the PDF. *Moderate* and *weak* magnetic fields tend to reduce the degree of fragmentation but once a gravitational instability sets in, the fields are unlikely to stop further collapse and star formation (e.g., Ziegler 2005; Banerjee et al. 2006). In this case, the N-PDF shows a power-law tail due to the gravitational collapse of the supercritical cores. Moreover, a change in dominant geometry (4.), i.e., from filamentary to spherical, could also provide an explanation. Longitudinal filament collapse on parsec scales reduces the mass transfer rate and dense gas is then piled up (Toala et al. 2012).

All of the above proposed mechanisms to produce column density excess should apply for all types of clouds – not only to the most massive GMCs. Therefore, high column density excesses should be observed more commonly, but this is not the case. Note, however, that the slope of the power-law tail(s) depends on the projection, i.e. the viewing angle, in which the cloud is being observed (Ballesteros-Paredes et al. 2011). In any case, a major difference between clouds forming only low-mass stars and those with high-mass star-formation is stellar feedback (5.). For example, additional compression by *internal* ionization due to an ultra-compact H II region can provoke a power-law tail with  $\alpha > 2$  (Tremblin et al. 2014). (High-mass) outflows may also play a role. It was shown by Sadavoy et al. (2014) that the slope of the power-law PDF in different regions in Perseus depends on the local feedback from low-mass young stellar objects. A recent study of MonR2 (Dierickx et al. 2015) revealed a significant number of CO outflows in the central region that imprints on the velocity structure of the region. Not all clouds with protostellar feedback, however, also show a second power-law. If feedback does not efficiently couple to the surroundings and the dense gas, an excess in the PDF might not develop or might not be visible at the observed scales in the column density PDF.

## 7 CONCLUSIONS AND OUTLOOK

At this point, it is not possible to give a final answer for our detection of excess/second power-law in the PDF of massive GMCs. Further studies are required to look into more

detail which of the proposed processes can play a dominant role. Besides more sophisticated 3D hydrodynamic simulations of star-forming regions a deeper understanding of how local thermal and dynamical properties are reflected in observations is needed.

## ACKNOWLEDGEMENTS

Part of this work was supported by the ANR-11-BS56-010 “STARFICH” and the ERC Grant 291294 “ORISTARS”. N.S. and V.O. acknowledge support by the DFG (Os 177/2-1 and 177/2-2) and central funds of the DFG-priority program 1573 (ISM-SPP).

## REFERENCES

- André, Ph., et al., 2014, PPVI, Univ. of Arizon Press, 914, p.27  
 Ballesteros-Paredes, et al., A., 2011, MNRAS, 416, 1436  
 Banerjee, R., Pudritz, R., Anderson, D., 2006, MNRAS, 373, 1091  
 Bohlin, R.C., Savage, B.D., Drake, J.F., 1978, ApJ 224, 132  
 Dierickx, M., Jimenez-Serra, I., et al., 2015, ApJ, 803, 89  
 Didelon, P., Motte, F., Tremblin, P., et al., 2015, A&A in press  
 Federrath, C., Klessen, R. S., 2013, ApJ, 763, 51  
 Froebrich, D., Rowles, J., 2010, MNRAS, 406, 1350  
 Fuente, A., Berné, O., Cernicharo, P. et al., 2010, A&A, 521, L23  
 Galvan-Madrid, R., Zhang, Q., et al., 2010, ApJ, 725, 17  
 Girichidis, P., et al., 2014, ApJ, 781, 91  
 Griffin, M., Abergel, A., Abreau, A., et al., 2010, A&A, 518, L3  
 Heitsch, F., et al., 2001, ApJ, 547, 280  
 Hennemann, M., Motte, F., et al., 2012, A&A, 543, L3  
 Hill, T., Motte F., Didelon P., et al., 2011, A&A, 533, 94  
 Hill, T., Motte F., Didelon P., et al., 2012, A&A, 542, 114  
 Kainulainen, J., Beuther, H., et al., 2009, A&A, 508, L35  
 Kainulainen, J., Beuther, H., et al., 2011, A&A, 530, 64  
 Klessen, R. S., 2000, ApJ, 535, 869  
 Könyves, V., André Ph., et al., 2015, A&A, in press  
 Koertgen, B., Banerjee, R., 2015, A&A sub., astro-ph: 1502.03306  
 Kritsuk, A.G., Norman, M.L., Wagner, R., 2011, ApJ, 727, L20  
 Krumholz, M., McKee, C., 2008, NATURE, 451, 1082  
 Larson, R.B., 2005, MNRAS, 359, L211  
 Motte, F., Zavagno A., Bontemps S., et al., 2010, A&A, 518, L77  
 Myers, P., 2015, ApJ, in press, astro-ph:1505.01124  
 Palmeirim, P., André, Ph., Kirk, J., et al., 2013, A&A, 550, 38  
 Peretto, N., Fuller, G.A., et al., 2013, A&A, 555, 112  
 Pilbratt, G., et al., 2010, A&A 518, L1  
 Poglitsch, A., Waelkens, C., Geis, N., et al., 2010, A&A 518, L2  
 Rivera-Ingraham, A., et al., 2015, ApJ, in press  
 Roccatagliata, V., Preibisch, T., et al., 2013, A&A, 554, 6  
 Roy, A., André, Ph., Palmeirim, P., et al., 2013, A&A,  
 Roy, A., Martin, P.G., Polychroni, D., et al., 2014, ApJ, 763, 55  
 Russeil, D., Schneider, N., et al., 2013, A&A, 554, 42  
 Sadavoy, S., Di Francesco, J., et al., 2014, ApJ, 787, L18  
 Schneider, N., Csengeri, T., et al., 2010, A&A, 520, 49  
 Schneider, N., Csengeri, T., et al., 2012, A&A, 540, L11  
 Schneider, N., André, P., Könyves, V., et al., 2013, ApJ, 766, L17  
 Schneider, N., Ossenkopf, V., et al., 2015a, A&A, 575, 79  
 Schneider, N., Csengeri, T., et al., 2015b, A&A, 578, 29  
 Toala, J.A., Vázquez-Semadeni, E., et al., 2012, ApJ, 744, 190  
 Tremblin, P., Schneider, N., et al., 2014, A&A, 564, 106  
 Vazquez-Semadeni, E., et al., 2008, MNRAS, 390, 769  
 Ziegler, U., 2005, A&A, 435, 385

This paper has been typeset from a  $\text{\LaTeX}$  file prepared by the author.